Original Research Article: full paper

(2022), «EUREKA: Physics and Engineering»
Number 4

CHARACTERIZATION OF WO_3 THIN FILMS DEPOSITED BY SPRAY PYROLYSIS TECHNIQUE AND ITS ROLE IN GAS SENSING

Sivaraman Sethu Sivathas[2]
Department of Physics[1]

Sambandam Murugan[2]
Department of Physics[1]

Arthur Victor Babu[2]✉
Department of Physics[1]
victornicy@gmail.com

Singaravelu Ramalingam[2]
Department of Physics[1]

Ramalingam Thirumurugan[2]
Department of Physics[1]

Devanugraham Clement Easter Raj Bernice Victoria
Department of Physics
TELC School of Higher Education
Pudukkottai, Tamil Nadu, India, 622001

[1]*A.V.C. College (Autonomous)*
Mannampandal, Mayiladuthurai, India, 609305

[2]*Bharathidasan University*
Tiruchirappalli, Tamil Nadu, India, 620024

✉**Corresponding author**

Abstract

The work investigated in this paper focused on the fabrication of WO_3 films by the spray pyrolysis technique, and different analyses were made to find optimized samples for studying properties suitable for the application of gas sensing. The substrate temperature is the most important parameter among other spray parameters for the synthesis of thin films hence WO_3 thin films were deposited on glass substrates by maintaining the substrate temperature at 350 °C, 450 °C, 550 °C, and 650 °C using compressed air as a carrier gas. The influence of the substrate temperature on the structural, morphological, compositional, and optical properties of the WO_3 thin films has been justified using XRD data. Good and enhanced crystallinity is observed for the film deposited at a substrate temperature of 550 °C. The nonconventional properties were studied by different investigations and confirmed by past research work. The manipulation of surface morphology with the different deposition temperatures is monitored. Only the characteristic peaks of W and O are present in the fabricated WO_3 thin films. The optical activity of about 70 to 80 % of the selected sample in the visible region (300 to 1200 nm) is found. The selective absorption activity of light in the ultraviolet region and visible region is checked. The obtained IR bands confirmed the inter bridge stretching and bending modes of W-O and O-W-O. A high response towards ammonia compared to other test gases is exhibited. The repeatability of WO_3 towards NH_3 over three periodic sensing cycles, response, and recovery time has also been discussed. From all the characteristic studies, it has been suggested that the fabricated WO_3 thin films have been used in the health care field to detect the toxic NH_3 gas.

Keywords: structural, morphological, compositional, optical, transparent, substrate, sensors, electrospray, crystallinity, deposition.

DOI: 10.21303/2461-4262.2022.002347

1. Introduction

In recent years, it is very important that, due to the development of populations, several sources are causing a huge impact on environmental and health issues. In this scenario, the

identification of unwanted sources releasing harmful gases against health and the sensing by detection of toxic gases have received increasing attention in recent years. Among toxic gases, ammonia (NH_3) is the important toxic gas that causes illness or heavy injury to the health environment of the human community when one inhales it through the eyes, nose, skin, and respiratory tract at high concentrations. NH_3 is generally exposed during the manufacturing of various industrial products, such as ice plants, bonding substances, automotive materials, and laboratory solvents. Furthermore, NH_3 is present in the inhaled breath of human beings and animals, which acts as a significant biomarker for the prognosis of kidney syndromes produced by the Helicobacter pylori bacterial stomach infection. The exhaled breath of patients with kidney syndromes and peptic ulcers releases NH_3 in the concentration range of 0.82 to 14.7 ppm. The seepage of combustible and volatile gases like ethanol, ammonia, and methanol causes massive accidents at elevated fuel [1]. Besides, NH_3 is produced in agricultural zones or by animal farming, which can affect the health of humans, wildlife, and the atmosphere. Hence, detection of NH_3 and monitoring are essential for life-saving, environmental shielding, and medical precautionary applications [2–5].

In this venture, there is a great need to prepare novel materials, particularly able semiconductor composites, for fabricating innovative gas sensors with rapid response and recovery times that can be used in extreme conditions. Numerous studies on metal oxide semiconductors like zinc oxide, tin oxide, indium oxide, tungsten oxide, molybdenum oxide, and vanadium oxide have been prepared and tested for the improvement of NH_3 gas sensors. Among them, WO_3 is an *n*-type semiconductor that is found to be a leading material for gas sensing applications. The sensing effects of WO_3 nanoparticles are determined by the ability of W ions to alter their valence state upon oxidation or reduction [6]. Tungsten trioxide (WO_3), a typical n-type semiconductor material with the usual bandgap ranging between 2.5 eV to 2.8 eV, has received a lot of interest for broad applications including photocatalysis, electrochromic devices, solar energy conversion, and gas sensors due to excellent catalytic, optical, and dielectric properties, and good physical and chemical stability. For gas sensing applications, WO_3 has attracted great attention for its distinctive sensing properties and has been regarded as a promising material for detecting various gases [7].

Between absolute zero and its melting point at 1700 K five distinct crystallographic modifications are adopted by tungsten trioxide. As the temperature is lowered from the melting point, WO_3 changes its crystallographic symmetry in the sequence: tetragonal-orthorhombic-monoclinic-triclinic-monoclinic. The functional properties of WO_3 are significantly improved by decreasing the size of the nanoscale [8] using constructing film morphology and improving the crystallographic texture of the film grains [9, 10]. The different structural, optical, and electrical behaviours of TO films depend on the deposition experimental conditions and techniques. The main factors which affect the films are the substrate temperature, the sputtering gas pressure, the flow properties of the TO rate, and the distance between the target and the substrate. These factors will disturb the physical parameters of the TO film as well as the tempering temperature, such as crystalline structure and optical transmittance, size of the TO, the density of the film, refractive index, etc., [11]. Tungsten trioxide finds its effective use in technical and industrial applications, and it can be deposited in thin film form by numerous deposition methods. Nowadays, WO_3 film has received great interest and anxiety concerning its outstanding gas-chromatic properties and has been recognized as one of the finest gas sensors for reducing gases. Deposition methods such as thermal evaporation, electron beam evaporation, chemical vapour deposition, sputtering, sol-gel, and spray pyrolysis have been employed to deposit tungsten trioxide thin films [12]. Each deposition method forms different properties on various substrates in terms of configuration, structure, and morphology [13, 14]. Spray pyrolysis is a simple and cost-effective technique for the deposition of the best quality, homogeneous, crystalline, and transparent thin films, and it is being used for large-area applications [15]. The most important parameters in deciding the properties of thin films are the deposition temperature. Hence, optimization of the preparative parameters during the formation of the metal oxide semiconductor (MOS) sensor is of prime importance. The deposition temperature affects the microstructural and morphological properties of the deposits. As far as the spray pyrolysis technique is concerned, the substrate temperature is the most important parameter among other spray parameters for the synthesis of thin films. In the present investigation, an

attempt was made to synthesize WO_3 thin films at different substrate temperatures (350 °C, 450 °C, 550 °C, 650 °C) using the Spray Pyrolysis Deposition technique for gas sensing applications.

2. Materials and Methods

2. 1. Synthesis of WO_3 thin Films

From the aqueous solutions containing 0.5M of WO_3 powder as a precursor, WO_3 thin films were deposited using compressed air as a carrier gas by the electrospray pyrolysis technique and the electrospray pyrolysis setup is shown in **Fig. 1.** A syringe needle is connected to a solution adjustable reservoir in the electrospray apparatus, and it is set aside at a distance of 8 cm from the reservoir to make sure that the pressurized mist spreads the hot substrate appropriately. To optimize the thickness, a different volume of precursor solution was sprayed and found to have a 500 nm film thickness. A trial-and-error method was used to verify the thickness of all samples. The substrate holder and syringe needle are connected to a high-voltage DC power supply, and the substrate holder is attached to a hot plate. Four sets of WO_3 thin films were deposited by maintaining the substrate temperatures at 350 °C, 450 °C, 550 °C, and 650 °C respectively. The optimal time of deposition, including the spray intervals for each sample, was found to be 44 min. The intermittent spray procedure was employed for 5 s and an interval of 10 s for each cycle.

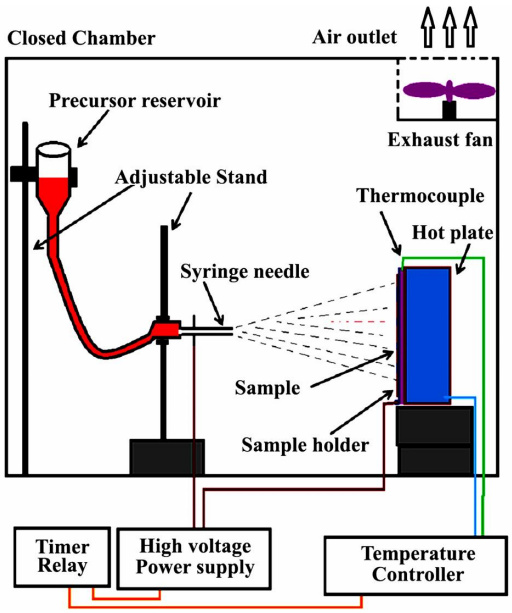

Fig. 1. Schematic diagram of the electrospray pyrolysis setup

2. 2. Characterization Techniques

An X-ray diffractometer (a SHIMADZU-XRD 6000 diffractometer system with an X-ray (Cu–Ka) wavelength of 1.5406) was used to examine the structural properties of the prepared WO_3 thin films. The SEM images were obtained by employing a scanning electron microscope (CARL ZEISS). XPS spectra are obtained by the K-Alpha X-ray Photoelectron spectrometer. The optical absorption and transparency of the films were measured in the wavelength range of 300 nm to 1100 nm using a Unico 4805 UV-Vis double beam spectrophotometer. The FTIR spectra were recorded using the SHIMADZU 1800-UV Fourier transform infrared spectrometer. Gas sensing measurements are made by a Keithley electrometer.

3. Results and Discussion

3. 1. XRD studies

Fig. 2 displays the XRD patterns of nano-WO_3 thin films that are deposited on glass substrates at different substrate temperatures. The XRD dispersive graph of the present material showed distinct peaks that agreed well with JCPDS card 43-1035, which confirmed the monoclinic

crystal structure. When looking at the XRD peaks at 350 °C and 450 °C, the peaks is found to be less intense, which is may be due to the poor agglomeration of the sub-planes of the crystal. This is mainly accomplished by the insufficient thermal energy to configure such a crystal. According to the previous study [16], it may also be due to the participated precursor being unable to work perfectly with electrochemical energy because also, the WO_3 crystal was aligned perfectly at 250 °C. The peak intensity of the sample at 550 °C was found to be high along with well-distributed and discrete signals. The respective peaks were observed at 23 °C, 24 °C, 26 °C, 30 °C, 34 °C, 42 °C, 52 °C, and 57 °C from (002), (020), (200), (112), (202), (222), (140), and (420) respectively. Except for the above peaks, there are several peaks observed that confirm an axis of a twofold symmetry system, and they are all assigned to the respective planes. Even though multiple peaks on XRD show an unpleasant crystal lattice atmosphere, the improved crystallinity behaviour is obtained at 550 °C. Some of the peaks with minimum intensity were observed which may be due to the occurrence of reciprocity in the crystal lattice structure. Usually, a reciprocal lattice is produced in the crystal due to the sharp subplanes and here, a similar trend is observed. Hence, at 650 °C the XRD peaks were observed to be analogous to those at 550 °C with minimum intensity. But the minimised energy peak showed a decomposed atmosphere of the crystal lattice. This condition in the XRD graph clearly shows the required thermal energy limitation for WO_3 materials. If the material has some dopant, the operating temperature may be changed. So, it is finally concluded that the optimized temperature of the WO_3 material is 550 °C.

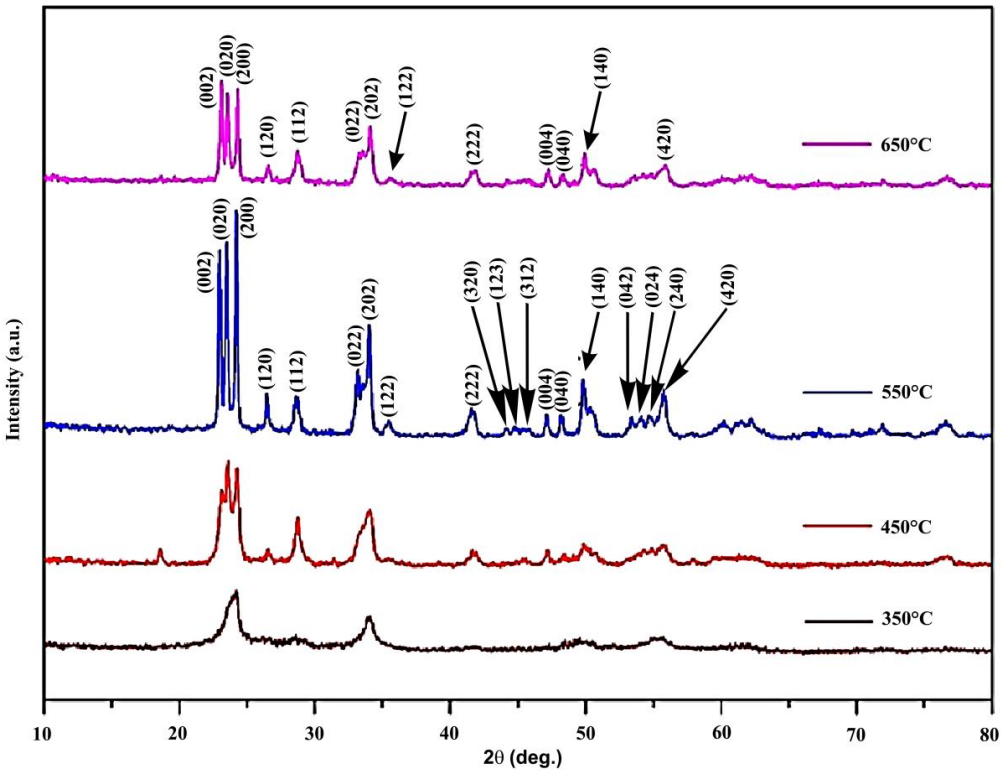

Fig. 2. X-Ray Diffraction spectra of WO_3 thin films deposited at various substrate temperature

3. 2. Particle size determination

The particle size of W is determined as usual by Debye-Scherrer's formulae for the active specific lattice. The data from the X-ray analysis are listed in **Table 1** to confirm the pattern of WO_3 thin film deposited temperatures at various substrate temperatures with calculated h, k, and l indices of the predominant peak in the (200) plane. The corresponding peak positions are 23.86, 23.78, 23.92, and 24.22, and the average particle size is calculated from a diffracted peak at 32.857 nm. At the initial state of temperature of 350 °C, the particle size is found to be 39 nm, which is moderate when compared with the literature. As the temperature is increased to 450 °C,

the particle size is found to be 36 nm, which is smaller than the previous one, and it is further decremented to 26 nm when the temperature is further increased to 550 °C. At this point of temperature, the reduction of size is stopped, and concerning WO_3, this is the λ point. Beyond this point, the nanoparticle efficiency is usually reduced, and this atmosphere takes place in this case also. In the case of microstrain, it increased from 350 °C to 550 °C and decreased further to 650 °C. It is very useful to explain the great order of crystallinity, and the good order is confirmed at 550 °C. For lattice strain, it is increased like microstrain, and normally it should be the opposite. This is obtained as a range between 0.004 and 0.0065, and, further, as 0.0058, about 650 °C. The d-spacing fluctuates in the range of 0.0122 to 0.0214 at 100 °C, which is due to the adverse effect of dynamic bonding forces, and it can be operated by a magnetic field also.

Table 1

XRD parameters of WO_3 thin films deposited at the various substrate temperature

Substrate temperature, °C	2θ	B	d-spacing	Particle size D, nm	Microstrain $\varepsilon\times10^{-3}$	Lattice strain Ξ
350	23.8658	0.2171	3.7270	39.077	0.926	0.0044
450	23.7872	0.2337	3.7392	36.326	0.995	0.0048
550	23.9256	0.3189	3.7178	26.65	1.361	0.0065
650	24.2266	0.2903	3.6723	29.375	1.234	0.0058

3. 3. SEM Examination

The SEM micrographs of WO_3 films deposited at various substrate temperatures (from 350 °C to 650 °C) are shown in **Fig. 3**. Form the SEM figure, it was clear that the surface morphology is found to vary with the different annealing temperatures. Initially, the sample at 350 °C, the surface morphology of the film was very rough and strapped in shape. In addition to that, some of the particles found with clear grain boundary. Similarly, the sample at 450 °C, the spherical shape particles appeared which abruptly explicit disorder of amalgamation whereas for the sample at 550 °C, well-shaped spherical particles are appeared and granulation with uniform distributed size morphology is observed. Finally, as the substrate temperature for the sample is raised to 650 °C, uneven morphology with an increase in grain size and a more porous surface is observed. The elevated and annealing energy beyond the limit enable the coalescence of the adjacent minute crystals, and therefore bulky surface grain boundary is determined [17]. So, the annealing temperature of 550 °C is the optimized annealing energy to enhance crystallinity. In addition to that, the drastic surface change was observed at every 100 °C of the material and the present nano material is highly sensitive even for every 5 °C of fluctuating temperature.

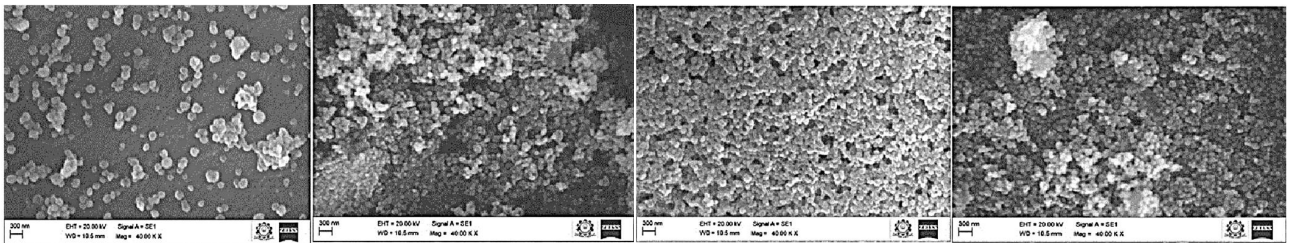

a *b* *c* *d*

Fig. 3. SEM images of WO_3 thin films deposited at substrate temperatures:
a – 350 °C; *b* – 450 °C; *c* – 550 °C; *d* – 650 °C

3. 4. XPS analysis

Using XPS measurements, the compositional characterization of WO_3 thin films deposited on the glass substrates is firmly decided. **Fig. 4** shows the XPS survey scan spectra of WO_3 thin film in the binding energy range of 0 to 1200 eV. The survey scan spectra are principally valuable for the recognition of the elements existing on the film's surface and inner core. The XPS spectra are the strong representation of partial elements of the WO_3 thin film, such as W and O.

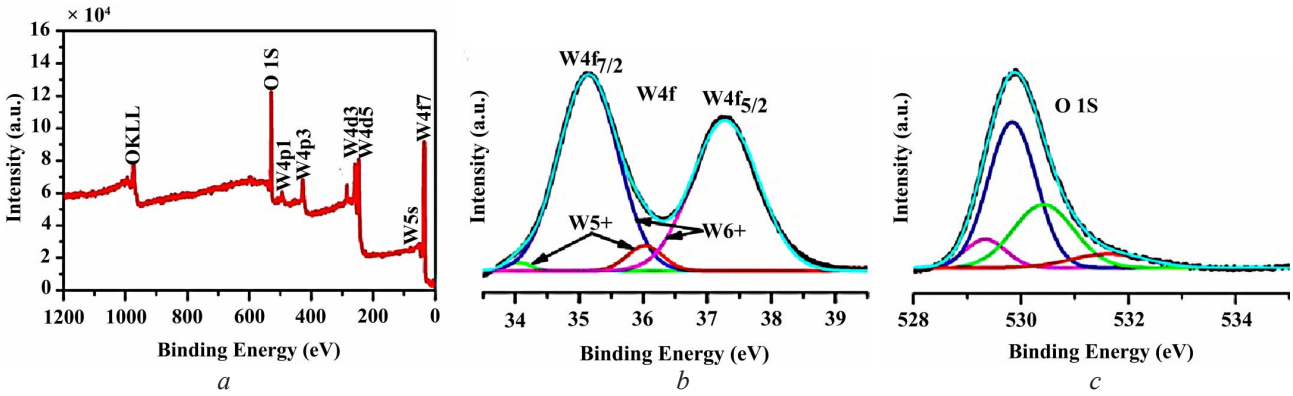

Fig. 4. XPS spectra of the WO_3 thin films:
a – XPS survey spectrum; *b* – the W4f spectrum; *c* – the O 1S spectrum

The first peak at 550 explores the presence of O, which is represented by the 1S orbital system. Furthermore, for as-deposited WO_3 thin films, to describe the ratio of O to W, the detailed scan spectrum is obtained for W4f and O1s. The spectra of W displayed in the figure show two main peaks ascribed to W4f7/2, and W4f5/2, which are positioned at 35.3 and 37.5 eV. The binding energy difference owing to spin-orbit splitting of W4f between W4f7/2 and W4f5/2 is found to be 2.20 eV. The XPS spectra of the O1s peak shown in the figure consist of two components: one at a binding energy of 530 eV, assigned to the oxygen in WO_3 films, and a smaller one at 532 eV, assigned to water molecules adsorbed on the film's surface [18]. The figure details the energy dispersion of W nanoparticles, which also reveals the existence of W nanoparticles in different spinning phases at molecular sites. The first spatial extension is represented by W_{5S}, the second is W_{d5}, the third is W_{d3}, the fourth is W_{P3}, and the fifth is W_{P1}. All the energy levels are obtained in different energy ranges, and all the energy ranges confirm the different energy bonding of WO_3 material in a thin film.

3. 5. Optical Properties

The optimized optical mechanism of WO_3 thin films at various substrate temperatures is depicted in **Fig. 5.** From the recorded spectra, it is observed that the transparency in the visible region ranges from 450 nm to 1200 nm with an optical transmittance of about 70 to 80 %. Transmittance increases with substrate temperature from 350 °C to 550 °C and then decreases at 650 °C, as expected. The maximum transmittance was obtained at 550 °C and this also showed the universal optimized annealing temperature range of WO_3 nanomaterial. The uniform oxygen vacancy generation over the surface-atmosphere demonstrates good light absorbance. The higher transmittance also confirmed the good crystalline nature of the material and that it is free from rational defects [19, 20].

The obtaining of broad bands in the optical absorption spectra of WO_3 is attributed to its wide optical absorption. Its coefficient of absorption is increased from low temperature to high temperature and it is stopped at 550 °C. From the figure, it is very clear that the absorption is initiated at 450 nm at 350 °C, whereas at 550 °C, the absorption efficiency started from 300 nm, which covers the UV region also. If the nanomaterial is efficient in the UV region, it will be more reactive for the assigned applications [21]. Here the same trend has appeared to explore the presently prepared nanomaterial.

The construction of visible region-driven semiconductor photocatalysts in nanomaterial is a very difficult process, and it is a very important issue in terms of harvesting photon energy for energy conversion. Usually, metal oxide nanomaterials have low efficiency and deal with the reduction of the recombination effect [22–24]. But, here, the energy band gap values range between 2.42 eV and 2.70 eV, according to which the band gap of the present material offers an efficient way to, address these limitations [25–27]. The band gap energy increases from 350 °C to 550 °C and at 650 °C, the band gap (2.60 eV) is reduced. The energy gap is

increased concerning the temperature and may also be due to the excessive formation of oxygen-ion vacancies in the films. The accurate band gap range is found to have opted to increase the photo efficiency.

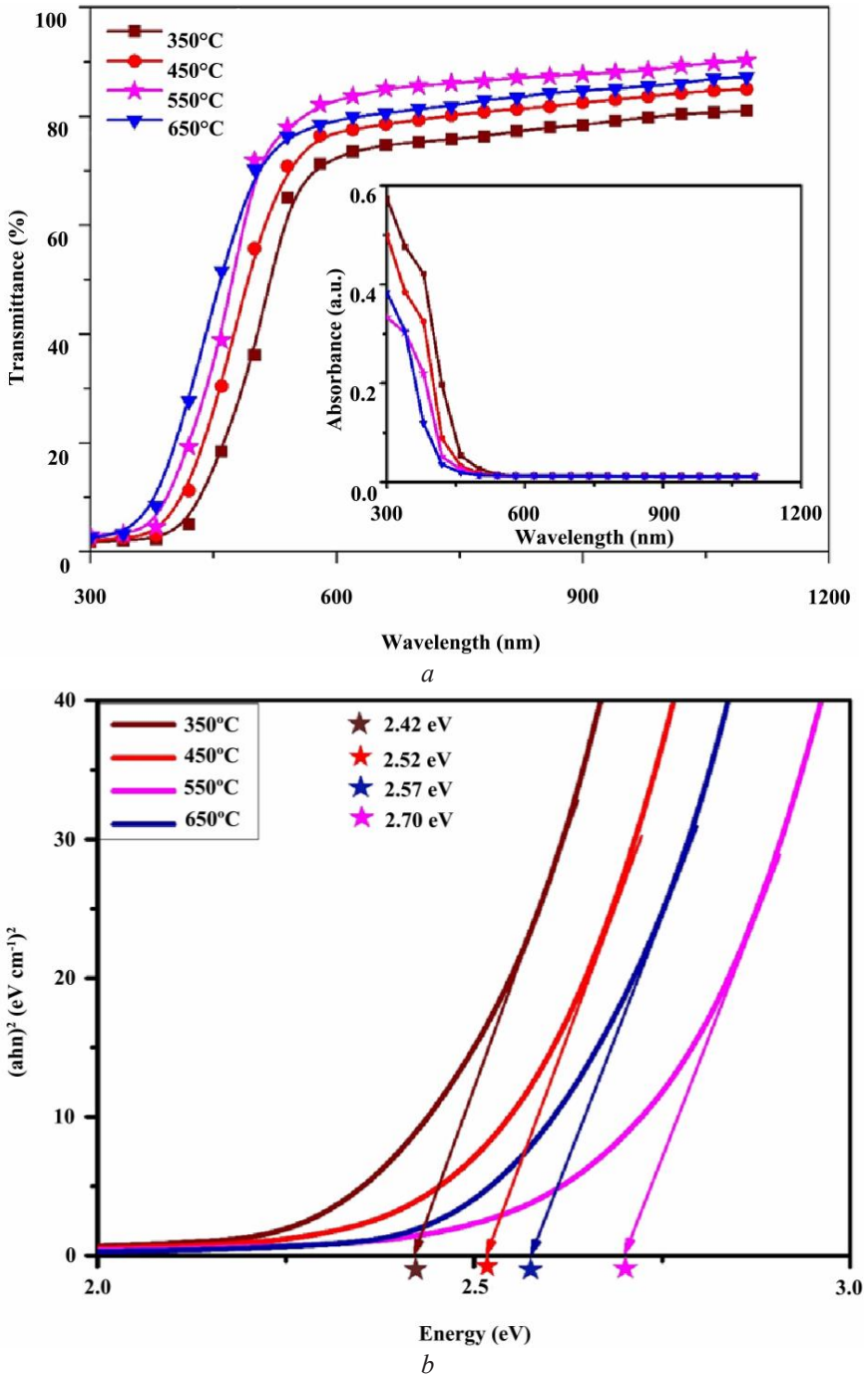

Fig. 5. UV-Visible Spectrum: *a* – transmittance and absorption spectra of WO_3 thin films; *b* – plot of $(\alpha h\upsilon)^2$ vs photon energy ($h\upsilon$) for WO_3 thin films

3. 6. FTIR analysis of WO_3 thin films

The presence of bonded elements in the material is usually represented by FTIR spectra of the samples and, concurrently, the spectra for all annealing temperatures are shown in **Fig. 6.** Since the binding energy is high for the inorganic components, the force constant will be high. The partial bonding involved in metal oxides is a very important factor that describes the elec-

trostatic forces that exist between the metal and the oxygen atom. Such interatomic bonding forces are always higher than ionic bonding. Here, for the present case of WO_3, the measured value is 18.122 a.u and it is very high for the nano crystal lattice, which is higher than bonding forces in the macro-molecular system. So, the respective frequencies of the bonds are very high when compared with the frequency observed for molecular level bonding. Usually, the IR bands appear for metal oxides in the region of 710 cm^{-1} to 550 cm^{-1} [28, 29]. In particular, the IR bands for W-O stretching bands are observed in the range of 680 cm^{-1} to 550 cm^{-1} [30]. The IR spectra for all prepared samples are shown in **Fig. 6**, in which a frequency shift of ±15 cm^{-1} is observed between the samples at different temperatures (350 °C to 650 °C). This may be due to the difference in the force constant of the W-O bond existing at different temperatures. Since the force constant of the W-O bond is 12.223 a.u the respective stretching vibrational frequency is obtained at 610 cm^{-1} with medium intensity for the sample at 350 °C. In such cases, the stretching frequency of the W-O bond for all cases is found at 610 with strong intensity. This is mainly due to the high force constant of the W-O bond (18.12 a.u.). The respective in-plane and out-of-plane bending modes are observed at 550 and 502 cm^{-1} in that order.

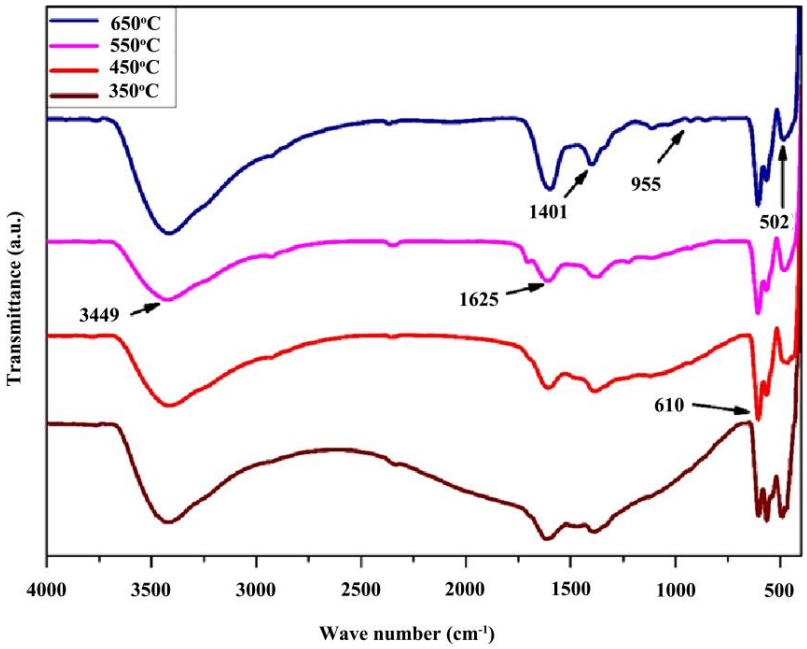

Fig. 6. FTIR spectra of the WO_3 thin films for various annealing temperatures

3. 7. Gas-Sensing Measurements

N–H bond identification is a very significant process for sensing ammonia gas. In this process, the N–H bonds of the gas are absorbed by the sensing material, and it affects the current carrying capacity by changing its resistance parameter. If this mechanism is easily adopted by the metal oxide material in a full-fledged manner, it will act as a good sensing material. The band gap as well as the gas absorption characteristics of the present case emphasized the gas sensing efficiency. **Fig. 7** shows the bar diagram of the device's response to different target gases at different temperatures. The sensing tests were performed to evaluate the selectivity of the sensor towards acetone, ammonia, ethanol, and formaldehyde; the results are portrayed in **Fig. 7**.

When compared to other samples, the WO_3 thin film deposited at a substrate temperature of 550 °C exhibits a high response to all gases. However, the film shows the lowest response to acetone, ethanol, and formaldehyde and exhibits the highest response to ammonia. The response of tungsten oxide to ammonia was taken for 1000 seconds, and that is shown in **Fig. 8.**

When the duration of absorption increases, the response value of the sensor uniformly increases. From the trail of the response time of the sensor, the linear fit curve was drawn, and from the fitting curve, its coefficient was determined to be 0.98927. To estimate the order of detection, NH_3 gas concentration has been tested from 5 ppm to 200 ppm, as shown in **Fig. 9**.

Upon exposure to NH_3 gas, the resistance decreases and when exposed to air, it is raised to its maximum, which indicates the *n*-type sensing behavior. As the concentration increases, the resistance decreases and the result indicates that the material is capable of offering good performance in gas sensing fields. The repeatability test is carried out for a particular sample and it is displayed in **Fig. 10**.

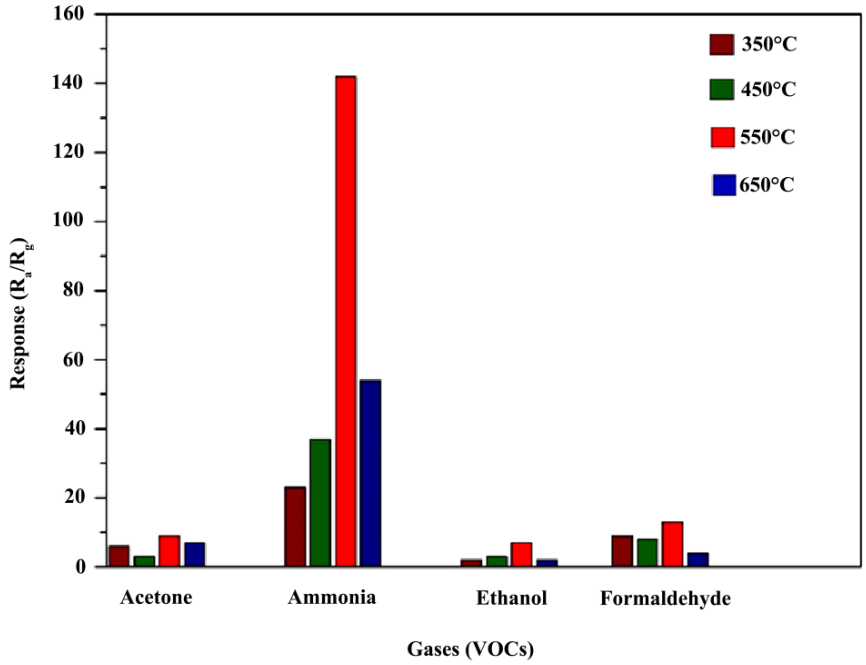

Fig. 7. The responses of sensors for different substrate temperatures

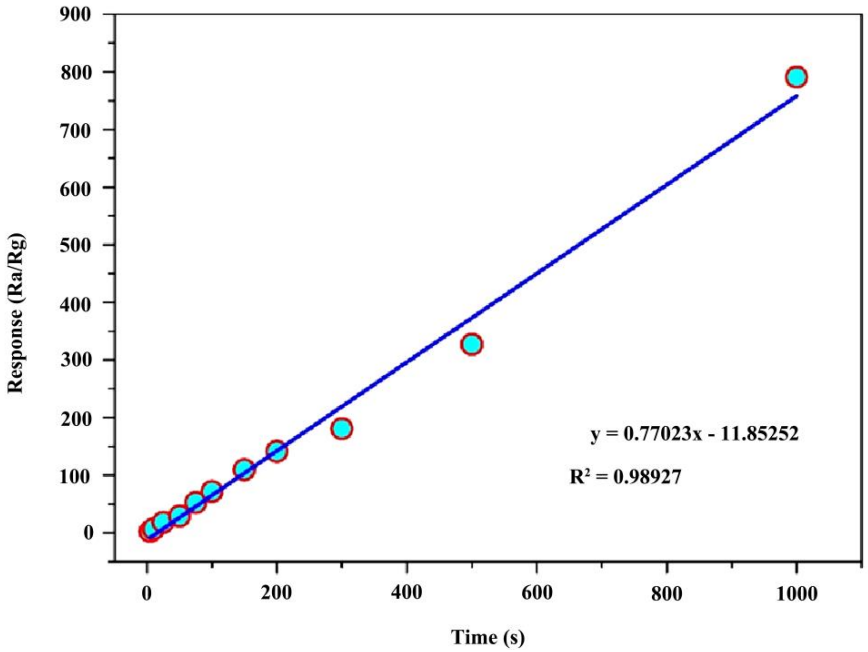

Fig. 8. The response linear fitting curve of the WO_3 sensor

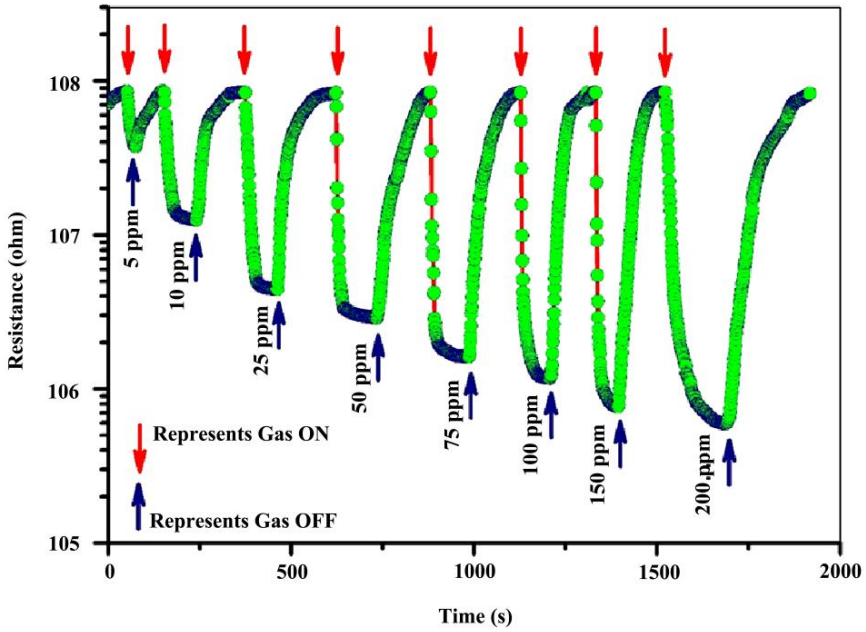

Fig. 9. Transient response characteristics of WO_3 sensor

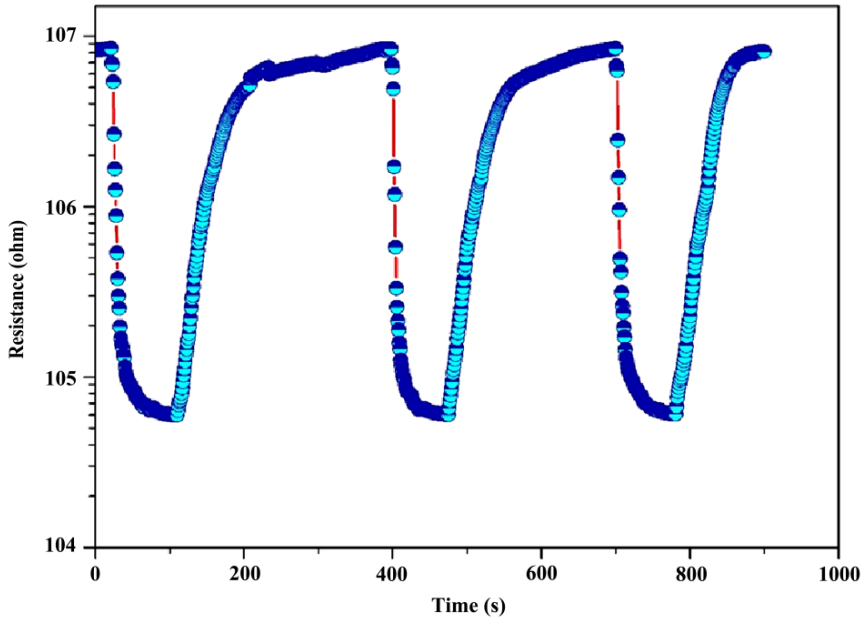

Fig. 10. The repeatability of the WO_3 sensor

3. 8. The response and recovery time of WO_3

The response and response/recovery time are both important parameters in evaluating a gas sensor's performance. It is evident from the earlier discussion that the films annealing above 550 °C resulted in the cracking of the films. As a result, the investigation of the response of the films is limited to those annealed at 550 °C. The repeatability of WO_3 towards NH_3 over three periodic sensing cycles is shown in **Fig. 10.** The sensor exhibits an almost stable response upon repeated exposure to NH_3, confirming the excellent repeatability of the sensor material suitable for automotive antipollution systems. The response and response/recovery time are both important parameters in evaluating a gas sensor's performance.

High response and fast response/recovery time could make the sensor an excellent candidate for the rapid detection of hazardous gases [31]. The response and recovery times are defined as

the time taken by the sensor to achieve 90 % of the total resistance change in the case of adsorption and desorption, respectively [32], and the response and recovery time under 550 °C towards 200 ppm is illustrated in **Fig. 11.** The response and recovery processes of the WO_3 sensing layer towards NH_3 are the results of thermally activated chemical reaction processes on the surface, with a response time of 27 s and recovery time of 77 s. This proves a very rapid process of gas absorption and response mechanism taking place in the WO_3 material. In the repetition curve, the saturation of resistance concerning time is considerably decreased. That showed the rapid response of the material to the gas absorption.

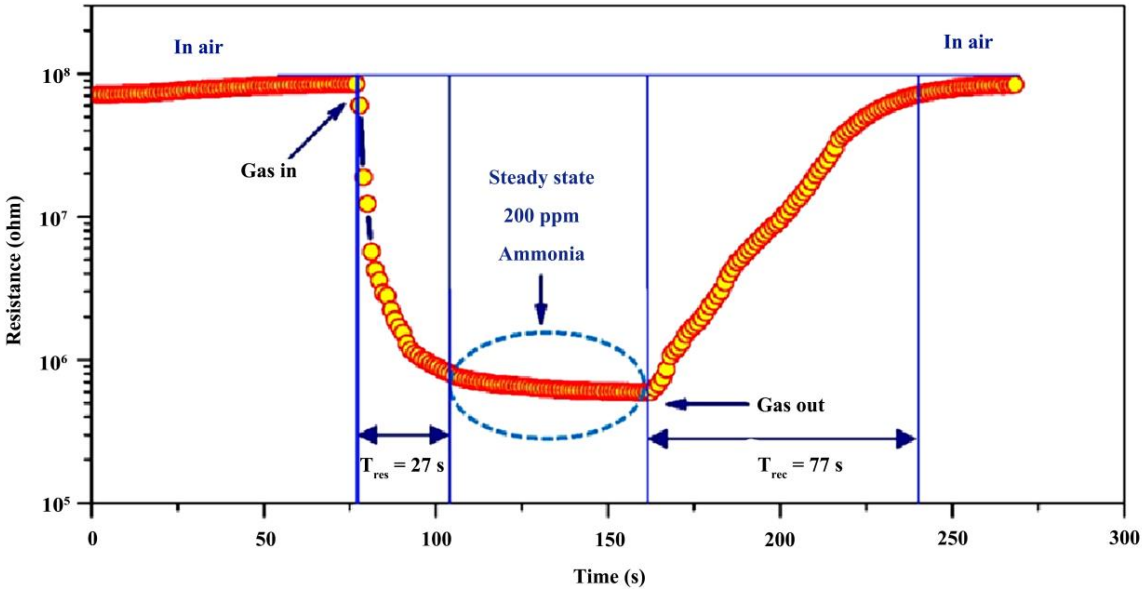

Fig. 11. The response and recovery time of the WO_3 gas sensor

3. 9. Limitations and the future scope of the study

Temperature plays a vital role in the deposition process of thin film deposition process, WO_3 Films deposited by means of a lower deposition temperature of below 350 °C give rise to irregular films due to the inadequate electrostatic attraction on the spray droplets hence WO_3 thin films deposited at the substrate temperature from 350 °C to 650 °C are characterized. Spray distance affects the quality of the deposited films hence the distance of the syringe needle is adjusted up and down and set aside at a distance of 8 cm from the reservoir and made sure that the pressurized mist spreads the hot substrate appropriately to obtain a continuous thin film.

In this work, the famous metal oxide WO_3 as thin film was prepared and characterized in order to study the assorted applications. The significant results have been traced abruptly and showed the improved application of metal oxide. In order to fulfill the future needs of advanced thin-film materials, the present thin-film material is to be modified further. For that, it is doped with d-block and f-block elements.

4. Conclusion

In this work, in order to prove the efficiency of the nano WO_3 material, the same has been prepared and the sample blended with suitable solvent coated as a thin film by the spray pyrolysis technique by maintaining the substrate temperature at 350 °C, 450 °C, 550 °C, and 650 °C, respectively. Each and every characterization analysis (morphological, structural, compositional, and optical) proved the efficiency of the prepared samples. As the substrate temperature is built to 550 °C, the crystalline nature of the film in the preferred plane orientation confirms the monoclinic phase of WO_3, and spherical-shaped particles have granulation with uniformly distributed size morphology are observed. The high-resolution XPS spectra of WO_3 exhibit two main peaks attributed to W4f7/2, and W4f5/2 centered at binding energy values of 35.3 and 37.5 eV. The efficiency is

manipulated by the application of annealing energy as temperature, and all the results validated that the properties are strongly influenced by the temperature. The prepared sample has been analyzed by changing annealing energy to optimize the well crystallinity of WO_3 material for gas sensing applications. Based on the observed results, the prepared material is having good optical, chemical and physical characteristics to make seed material for manufacturing advanced sensor devices. The vibrational spectra of the samples confirm the W-O bond in the material. The in-plane and out-of-plane bending modes ensure the bond angle of O-W-O of WO_3, which exhibits the highest response towards ammonia gas. Hence, by this work, it is suggested that the fabricated WO_3 thin films have been used in the health care field to detect toxic NH_3 gas, which causes immediate burning of the eyes, nose, throat, and respiratory tract, which results in blindness, lung damage, or even death.

References

[1] Sun, L., Han, C., Wu, N., Wang, B., Wang, Y. (2018). High temperature gas sensing performances of silicon carbide nanosheets with an n–p conductivity transition. RSC Advances, 8 (25), 13697–13707. doi: https://doi.org/10.1039/c8ra02164c

[2] Li, H.-Y., Lee, C.-S., Kim, D. H., Lee, J.-H. (2018). Flexible Room-Temperature NH_3 Sensor for Ultrasensitive, Selective, and Humidity-Independent Gas Detection. ACS Applied Materials & Interfaces, 10 (33), 27858–27867. doi: https://doi.org/10.1021/acsami.8b09169

[3] Naseem, S., King, A. J. (2018). Ammonia production in poultry houses can affect health of humans, birds, and the environment-techniques for its reduction during poultry production. Environmental Science and Pollution Research, 25 (16), 15269–15293. doi: https://doi.org/10.1007/s11356-018-2018-y

[4] Seekaew, Y., Pon-On, W., Wongchoosuk, C. (2019). Ultrahigh Selective Room-Temperature Ammonia Gas Sensor Based on Tin-Titanium Dioxide/reduced Graphene/Carbon Nanotube Nanocomposites by the Solvothermal Method. ACS Omega, 4 (16), 16916–16924. doi: https://doi.org/10.1021/acsomega.9b02185

[5] Fedoruk, M. J., Bronstein, R., Kerger, B. D. (2005). Ammonia exposure and hazard assessment for selected household cleaning product uses. Journal of Exposure Science & Environmental Epidemiology, 15 (6), 534–544. doi: https://doi.org/10.1038/sj.jea.7500431

[6] Jeevitha, G., Abhinayaa, R., Mangalaraj, D., Ponpandian, N., Meena, P., Mounasamy, V., Madanagurusamy, S. (2019). Porous reduced graphene oxide (rGO)/WO_3 nanocomposites for the enhanced detection of NH_3 at room temperature. Nanoscale Advances, 1 (5), 1799–1811. doi: https://doi.org/10.1039/c9na00048h

[7] Lu, R., Zhong, X., Shang, S., Wang, S., Tang, M. (2018). Effects of sintering temperature on sensing properties of WO_3 and Ag-WO_3 electrode for NO_2 sensor. Royal Society Open Science, 5 (10), 171691. doi: https://doi.org/10.1098/rsos.171691

[8] Hassel, A. W., Smith, A. J., Milenkovic, S. (2006). Nanostructures from directionally solidified NiAl–W eutectic alloys. Electrochimica Acta, 52 (4), 1799–1804. doi: https://doi.org/10.1016/j.electacta.2005.12.061

[9] Blackman, C. S., Parkin, I. P. (2005). Atmospheric Pressure Chemical Vapor Deposition of Crystalline Monoclinic WO_3 and WO_3-x Thin Films from Reaction of WCl6 with O-Containing Solvents and Their Photochromic and Electrochromic Properties. Chemistry of Materials, 17 (6), 1583–1590. doi: https://doi.org/10.1021/cm0403816

[10] Ashraf, S., Binions, R., Blackman, C. S., Parkin, I. P. (2007). The APCVD of tungsten oxide thin films from reaction of WCl_6 with ethanol and results on their gas-sensing properties. Polyhedron, 26 (7), 1493–1498. doi: https://doi.org/10.1016/j.poly.2006.11.017

[11] Qadri, M. U., Pujol, M. C., Ferré-Borrull, J., Llobet, E., Aguiló, M., Díaz, F. (2011). WO_3 thin films for optical gas sensing. Procedia Engineering, 25, 260–263. doi: https://doi.org/10.1016/j.proeng.2011.12.064

[12] Rao, M. C. (2011). Effect of substrate temperature on the structural and electrical conduction behaviour of vacuum evaporated WO_3 thin films. Journal of Optoelectronics and Biomedical Materials, 3 (2), 45–50. Available at: https://chalcogen.ro/45_Rao.pdf

[13] Hussain, O. M., Swapnasmitha, A. S., John, J., Pinto, R. (2005). Structure and morphology of laser-ablated WO3 thin films. Applied Physics A, 81 (6), 1291–1297. doi: https://doi.org/10.1007/s00339-004-3041-z

[14] Soto, G. (2003). Characterization of tungsten oxide films produced by reactive pulsed laser deposition. Applied Surface Science, 218 (1-4), 282–290. doi: https://doi.org/10.1016/s0169-4332(03)00677-9

[15] Vardhan, R. V., Kumar, S., Mandal, S. (2020). A facile, low temperature spray pyrolysed tungsten oxide (WO_3): an approach to antifouling coating by amalgamating scratch resistant and water repellent properties. Bulletin of Materials Science, 43 (1). doi: https://doi.org/10.1007/s12034-020-02250-z

[16] Hasan, S. F., Al-Samarai, A.-M. E., Obaid, A. S., Ramizy, A. (2021). Study the Structure and Optical Properties of GNPs Doped WO_3/PS by Spray Pyrolysis Deposition (SPD). IOP Conference Series: Materials Science and Engineering, 1095 (1), 012011. doi: https://doi.org/10.1088/1757-899x/1095/1/012011

[17] Liang, Y.-C., Chang, C.-W. (2019). Preparation of Orthorhombic WO_3 Thin Films and Their Crystal Quality-Dependent Dye Photodegradation Ability. Coatings, 9 (2), 90. doi: https://doi.org/10.3390/coatings9020090

[18] Patel, K. J., Bhatt, G. G., Patel, S. S., Desai, R. R., Ray, J. R., Panchal, C. J. et. al. (2017). Thickness-dependent Electrochromic Properties of Amorphous Tungsten Trioxide Thin Films. Journal of Nano- and Electronic Physics, 9 (3), 03040. doi: https://doi.org/10.21272/jnep.9(3).03040

[19] Beena, D., Lethy, K. J., Vinodkumar, R., Mahadevan Pillai, V. P., Ganesan, V., Phase, D. M., Sudheer, S. K. (2009). Effect of substrate temperature on structural, optical and electrical properties of pulsed laser ablated nanostructured indium oxide films. Applied Surface Science, 255 (20), 8334–8342. doi: https://doi.org/10.1016/j.apsusc.2009.05.057

[20] Bujji Babu, M., Madhuri, K. (2017). Structural, morphological and optical properties of electron beam evaporated WO_3 thin films. Journal of Taibah University for Science, 11 (6), 1232–1237. doi: https://doi.org/10.1016/j.jtusci.2016.12.003

[21] Sivakumar, R., Gopalakrishnan, R., Jayachandran, M., Sanjeeviraja, C. (2007). Preparation and characterization of electron beam evaporated WO_3 thin films. Optical Materials, 29 (6), 679–687. doi: https://doi.org/10.1016/j.optmat.2005.11.017

[22] An, X., Yu, J. C., Wang, Y., Hu, Y., Yu, X., Zhang, G. (2012). WO_3 nanorods/graphene nanocomposites for high-efficiency visible-light-driven photocatalysis and NO_2 gas sensing. Journal of Materials Chemistry, 22 (17), 8525. doi: https://doi.org/10.1039/c2jm16709c

[23] Bai, S., Zhang, K., Sun, J., Luo, R., Li, D., Chen, A. (2014). Surface decoration of WO_3 architectures with Fe_2O_3 nanoparticles for visible-light-driven photocatalysis. CrystEngComm, 16 (16), 3289. doi: https://doi.org/10.1039/c3ce42410c

[24] Bi, D., Xu, Y. (2013). Synergism between Fe_2O_3 and WO_3 particles: Photocatalytic activity enhancement and reaction mechanism. Journal of Molecular Catalysis A: Chemical, 367, 103–107. doi: https://doi.org/10.1016/j.molcata.2012.09.031

[25] Li, X., Lin, H., Chen, X., Niu, H., Liu, J., Zhang, T., Qu, F. (2016). Dendritic α-Fe_2O_3/TiO_2 nanocomposites with improved visible light photocatalytic activity. Physical Chemistry Chemical Physics, 18 (13), 9176–9185. doi: https://doi.org/10.1039/c5cp06681f

[26] Ramos-Delgado, N. A., Gracia-Pinilla, M. A., Maya-Treviño, L., Hinojosa-Reyes, L., Guzman-Mar, J. L., Hernández-Ramírez, A. (2013). Solar photocatalytic activity of TiO_2 modified with WO_3 on the degradation of an organophosphorus pesticide. Journal of Hazardous Materials, 263, 36–44. doi: https://doi.org/10.1016/j.jhazmat.2013.07.058

[27] Riboni, F., Bettini, L. G., Bahnemann, D. W., Selli, E. (2013). WO_3–TiO_2 vs. TiO_2 photocatalysts: effect of the W precursor and amount on the photocatalytic activity of mixed oxides. Catalysis Today, 209, 28–34. doi: https://doi.org/10.1016/j.cattod.2013.01.008

[28] Jothibas, M., Manoharan, C., Ramalingam, S., Dhanapandian, S., Johnson Jeyakumar, S., Bououdina, M. (2013). Preparation, characterization, spectroscopic (FT-IR, FT-Raman, UV and visible) studies, optical properties and Kubo gap analysis of In_2O_3 thin films. Journal of Molecular Structure, 1049, 239–249. doi: https://doi.org/10.1016/j.molstruc.2013.06.047

[29] Ayeshamariam, A., Ramalingam, S., Bououdina, M., Jayachandran, M. (2014). Preparation and characterizations of SnO_2 nanopowder and spectroscopic (FT-IR, FT-Raman, UV–Visible and NMR) analysis using HF and DFT calculations. Spectrochimica Acta Part A: Molecular and Biomolecular Spectroscopy, 118, 1135–1143. doi: https://doi.org/10.1016/j.saa.2013.09.030

[30] Socrates, G. (2001). Infrared and Raman Characteristic Group Frequencies: Tables and Charts. Wiley, 366. Available at: https://books.google.com.ua/books/about/Infrared_and_Raman_Characteristic_Group.html?id=lOx9QgAACAAJ&redir_esc=y

[31] Li, Y., Chen, N., Deng, D., Xing, X., Xiao, X., Wang, Y. (2017). Formaldehyde detection: SnO_2 microspheres for formaldehyde gas sensor with high sensitivity, fast response/recovery and good selectivity. Sensors and Actuators B: Chemical, 238, 264–273. doi: https://doi.org/10.1016/j.snb.2016.07.051

[32] Zhao, Y.-F., Sun, Y.-P., Yin, X., Yin, G.-C., Wang, X.-M., Jia, F.-C., Liu, B. (2018). Effect of Surfactants on the Microstructures of Hierarchical SnO_2 Blooming Nanoflowers and their Gas-Sensing Properties. Nanoscale Research Letters, 13 (1). doi: https://doi.org/10.1186/s11671-018-2656-5

Received date 20.04.2022
Accepted date 11.07.2022
Published date 30.07.2022

How to cite: *Sivathas, S. S., Murugan, S., Babu, A. V., Ramalingam, S., Thirumurugan, R., Victoria, D. C. E. R. B. (2022). Characterization of WO_3 thin films deposited by spray pyrolysis technique and its role in gas sensing. EUREKA: Physics and Engineering, 4, 101–113. https://doi.org/10.21303/2461-4262.2022.00*